Mechanics and Materials Center
TEXAS A&M UNIVERSITY
College Station, Texas

AD-A233 031

AFOSR-TR. 01 0194

DEFORMATION AND FRACTURE OF FIBER-REINFORCED
CERAMIC COMPOSITES

FINAL TECHNICAL REPORT

R. A. SCHAPERY

AIR FORCE OFFICE OF SCIENTIFIC RESEARCH
OFFICE OF AEROSPACE RESEARCH
UNITED STATES AIR FORCE
GRANT NO. AFOSR-90-0028

MM-27470-90-15   DECEMBER 1990

91 3 08 045

REPORT DOCUMENTATION PAGE

Form Approved
OMB No. 0704-0188

1a. REPORT SECURITY CLASSIFICATION	1b. RESTRICTIVE MARKINGS
unclassified	

2a. SECURITY CLASSIFICATION AUTHORITY	3. DISTRIBUTION/AVAILABILITY OF REPORT
	Approved for public release,
2b. DECLASSIFICATION/DOWNGRADING SCHEDULE	distribution unlimited

4. PERFORMING ORGANIZATION REPORT NUMBER(S)	5. MONITORING ORGANIZATION REPORT NUMBER(S)
MM-27470-90-15	

6a. NAME OF PERFORMING ORGANIZATION	6b. OFFICE SYMBOL (If applicable)	7a. NAME OF MONITORING ORGANIZATION
Mechanics and Materials Center Texas A&M University		AFOSR/NA

6c. ADDRESS (City, State, and ZIP Code)	7b. ADDRESS (City, State, and ZIP Code)
College Station, TX 77843	Building 410 Bolling AFB, DC 20332-6448

8a. NAME OF FUNDING/SPONSORING ORGANIZATION	8b. OFFICE SYMBOL (If applicable)	9. PROCUREMENT INSTRUMENT IDENTIFICATION NUMBER
AFOSR	NA	Grant No. AFOSR-90-0028

8c. ADDRESS (City, State, and ZIP Code)	10. SOURCE OF FUNDING NUMBERS			
	PROGRAM ELEMENT NO.	PROJECT NO.	TASK NO.	WORK UNIT ACCESSION NO.
Building 410 Bolling AFB, DC 20332-6448	61102F	2302	B2	

11. TITLE (Include Security Classification)
Deformation and Fracture of Fiber-Reinforced Ceramic Composites (u)

12. PERSONAL AUTHOR(S)
R.A. Schapery

13a. TYPE OF REPORT	13b. TIME COVERED	14. DATE OF REPORT (Year, Month, Day)	15. PAGE COUNT
Final	FROM 10/1/89 TO 8/31/90	December 1990	20 + Appendix

16. SUPPLEMENTARY NOTATION

17. COSATI CODES			18. SUBJECT TERMS (Continue on reverse if necessary and identify by block number)
FIELD	GROUP	SUB-GROUP	Ceramic Composites Fiber-Reinforced Ceramics
			Composites Viscoelasticity
			Delamination Crack Growth

19. ABSTRACT (Continue on reverse if necessary and identify by block number)

Theoretical work on crack and damage growth in ceramic composites is summarized. Micromechanical models for viscoelastic behavior and crack growth in ceramics with a viscous grain boundary phase are developed. The emphasis is on extending earlier work for the limiting cases of elastic or viscous behavior to realistic viscoelastic behavior. Relationships for creep functions and crack speed are derived. Predictions for creep of ceramics with growing microcracks are made and compared with some experimental data. A publication on delamination analyisis is in the appendix.

20. DISTRIBUTION/AVAILABILITY OF ABSTRACT	21. ABSTRACT SECURITY CLASSIFICATION
☑ UNCLASSIFIED/UNLIMITED ☑ SAME AS RPT. ☐ DTIC USERS	unclassified

22a. NAME OF RESPONSIBLE INDIVIDUAL	22b. TELEPHONE (Include Area Code)	22c. OFFICE SYMBOL
LTC Steven C. Boyce	(202) 767-0103	NA

DD Form 1473, JUN 86   Previous editions are obsolete.   SECURITY CLASSIFICATION OF THIS PAGE

1. RESEARCH OBJECTIVE

The overall objective of the proposed research is to use experimental and theoretical studies to develop models for the thermomechanical behavior of ceramic fiber-reinforced ceramic matrix composites. Types, severity and growth mechanisms of damage in composites under simple and complex stress and temperature histories will be characterized experimentally. Theoretical models will be developed for thermomechanical response in terms of microstructural parameters, such as grain size, fiber diameter and orientation, volume fraction of fibers, porosity, interfacial fracture resistance as well as the micromechanics of damage growth.

2. ACCOMPLISHMENTS

2.1 Overview

Theoretical work during the past year was concerned with (1) damage growth in ceramic matrices at high temperature and with (2) mixed-mode delamination. Improved understanding of both types of damage is needed in order to predict thermomechanical behavior of ceramic composite laminates.

Under item (1), models of crack and damage growth were developed which account for both <u>elastic</u> behavior of crystalline grains and <u>viscous</u> behavior of grain boundary phases. These results for <u>viscoelastic behavior</u> generalize earlier work of others which appears to be limited to the extremes of elastic behavior and viscous behavior. This analysis has not yet been published, and therefore

essential features of the theory and some results are given in the body of this report in Section 2.2

Item (2) on delamination was written and published during the grant period [1]; the publication is in the Appendix. It represents a departure from other formulations of mixed-mode delamination analysis. Traditionally, the total energy release rate and its components have been expressed in terms of moments and forces acting on the boundaries of the crack (delamination) tip element (cf. Fig. 3, Appendix). Instead, we developed the energy release rates directly in terms of crack tip moments and forces. This approach leads to simpler results, especially for complex layups, and simplifies the analytical or numerical methods needed for computing mode ratios. Some further work on the prediction of mode ratios and on the effects of temperature and shear deformations is currently underway.

Experimental studies were not started because of the departure of the co-principal investigator, Professor M. C. Lu, from Texas A&M University (shortly after the grant was awarded) and Professor Schapery's intention to move to The University of Texas at Austin near the end of the first year of the grant. It is planned to initiate the experimental work at The University of Texas at Austin as soon as personnel and equipment are available.

2.2 Damage Growth in Viscoelastic Ceramics

2.2.1. **Background.** An important micromechanism for time-dependent deformation in many ceramics and ceramic composites is the nucleation, growth and coalescence of cavities and crack-like defects along grain boundaries and interfaces [2]. Amorphous phases that are often present along grain boundaries and interfaces are usually modeled as linear or nonlinear viscous materials (i.e., the current shear stress is a function of the current shear strain rate), and we shall do so here. The objective of the present analysis is to develop a model for predicting the growth of individual cracks in viscous, cavitating grain boundaries or interfaces and to use this model to predict the effect of a distribution of such cracks on the global behavior of polycrystalline ceramics.

The primary background references for this work are the crack tip model of Thouless et al. [3], the distributed damage model of Suresh and Brockenbrough [2], and the viscoelastic crack growth theory of Schapery [4]. In [2] the effect of the growth of distributed damage on creep of ceramics and ceramic composites is predicted using results from [3] for crack growth rate.

Let us first review certain aspects of these two important studies before discussing the new theory. Figure 1 shows the crack tip model of [3], in which the cavities grow and coalesce in a very thin viscous layer between essentially rigid grains. The "viscous matrix" outside of the damage zone represents the undamaged, surrounding, deformable polycrystalline material. Grain

deformations, in effect, are neglected inside and outside of the damage zone. The undamaged continuum deforms through straining of the viscous grain boundaries.
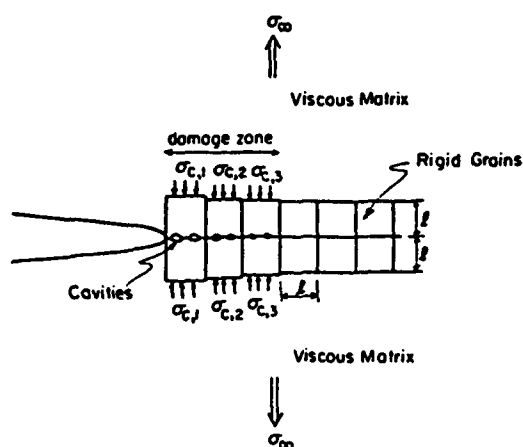

Fig. 1. The theoretical situation considered in [3]. The damage zone consists of an array of grains co-planar with the crack and embedded in a linearly viscous matrix. The growth of cavities is constrained by the viscous matrix.

The result for crack speed å may be written obtained in the form

$$\text{å} = \frac{K_I \sqrt{d}}{\eta} \, G^*(d/\lambda, \, \alpha/d, \, A_f) \qquad (1)$$

where

K_I	=	opening-mode stress intensity factor
d	=	grain size
α	=	length of damage zone ($\alpha \geq d$)
η	=	viscosity of grain boundary phase
λ	=	cavity spacing ($d/\lambda > 1$)
A_f	=	critical area fraction of cavitated grain boundary at which cavities coalesce (for the grain at the crack tip)
G^*	=	dimensionless function

Graphs of the theoretically predicted function G* are given in [3].

It is of particular interest to observe that crack speed is proportional to K and $\sqrt{d}$ and inversely proportional to η. This behavior could have been predicted directly from dimensional analysis (for the material and geometry idealizations assumed), although this approach was not used in [3]. Rather, a detailed analysis was employed which not only provided these dependencies but also gave the function G* (graphically, in most cases).

Suresh and Brockenbrough [2] used the linear relationship between $\dot{a}$ and K_I to predict the creep of ceramics when all of the creep is due to distributed microcrack (damage) growth. They concluded that for short time behavior the strain rate $\dot{\epsilon}$ is proportional to K_I^2 and therefore

$$\dot{\epsilon} \sim \sigma^2 \qquad (2)$$

Prediction and experimental results for polycrystalline alumina and alumina-silicon carbide composite are shown in Fig. 2; their theory gives the straight lines with a slope of two in the figure.

However, in [2] the ceramic was assumed to be fully elastic (except for the viscous layer in each microcrack tip damage zone) whereas in [3] the ceramic's overall behavior was assumed to be viscous (with rigid grains). Had the assumption of viscous behavior been used in [2], the lines in Fig. 2 would have had a slope of unity instead of two, clearly at odds with the experimental data.
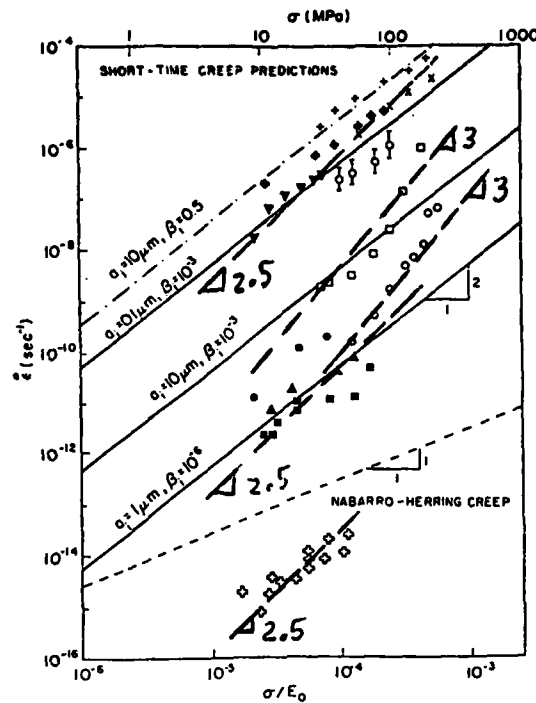
Fig. 2. Steady-state creep characteristics of polycrystalline alumina and alumina-silicon carbide composite. See [2] for details. The dark dashed lines come from the theory discussed in Section 2.2.4.

Here, we shall use elastic grains and a viscous grain boundary phase in **both** the crack tip and distributed damage models. This generalization will enable us to predict behavior which is in better agreement with the experimental data.

2.2.2. The Undamaged Polycrystalline Continuum. Both the crack tip model and the model for global material response with distributed damage require a constitutive equation for the undamaged portion of the ceramic. Linear viscoelastic behavior will be taken into account.

For a uniaxial stress, the axial strain for an arbitrary stress history $\sigma(\tau)$ is,

$$\epsilon = \int_{-\infty}^{t} D(t-\tau)\frac{d\sigma}{d\tau}\,d\tau$$

(3)

The quantity D(t) is the "creep compliance." For a creep test, in which the stress is applied at $\tau = 0$ and held constant thereafter, equation (3) yields

$$\epsilon = D(t)\sigma \qquad (4)$$

Thus, D(t) may be obtained from creep test data as $D = \epsilon/\sigma$ for t > 0; $D \equiv O$ for t < 0. Instead, here we shall predict D(t) as well as the associated creep Poison's ratio $v_c(t)$, using the micromechanical model shown in Fig. 3.

This model is usually called the "generalized self-consistent scheme" or the "three-phase model" in the context of particulate composites. The equations for the overall (or effective) elastic Young's modulus E and Poisson's ratio v are given in [5]. A grain is idealized here as a spherical particle and the grain boundary as a concentric matrix layer. A representative "two-phase composite" consisting of a grain and grain boundary phase is embedded in the third phase; the latter phase has the properties (E, v) the undamaged ceramic. These properties are predicted by requiring that E and v for the three-phase composite in Fig. 3 equal those for an effectively homogeneous material with the same E and v. The equations in [5] may be used to calculate these elastic constants in terms of:

E_m, E_p = matrix and particle Young's modulus, respectively.

v_m, v_p = matrix and particle Poisson's ratio, respectively.
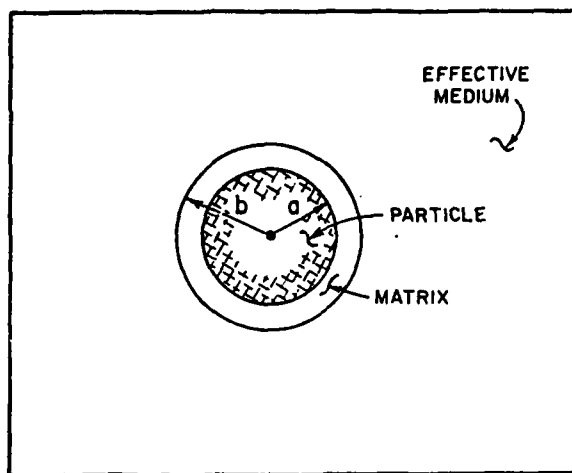
V_p = particle volume fraction

Fig. 3. Generalized self-consistent scheme without microcracking. The particle and matrix represent a grain and grain boundary phase, respectively.

In turn, the correspondence principle of linear viscoelasticity theory, along with Laplace transform inversion, enables us to predict from these elasticity results the creep functions $D(t)$ and $v_c(t)$ for a composite with viscoelastic constituents. Alternatively, approximate results for $D(t)$ and $v_c(t)$ may be found by the simpler quasi-elastic method [6], which we use here.

We assume the grains are elastic. The grain boundary phase (the matrix) is assumed elastic in dilatation (constant bulk modulus) and is a viscoelastic Maxwell model in shear,

$$J_m = J_{mo} + t/\eta_m \qquad (5)$$

where

J_m	$=$	shear creep compliance
J_{mo}	$=$	initial (elastic) value of shear creep compliance, which is the reciprocal of the initial shear modulus.
η_m	$=$	shear viscosity

Observe that at long times $(t \gg J_{mo}\eta_m)$ the grain boundary phase becomes a viscous material, while at short times it is elastic.

Figures 4 and 5 are graphs of the logarithms (base 10) of the plane-strain creep compliance $C(t)$ of the polycrystalline ceramic material versus time, where

$$T_o = J_{mo}\eta, \text{ the creep time constant}$$

$$C = [1 - v_c^2(t)] \, D(t) \qquad (6)$$

and C_o is the initial value of C. The plane-strain creep compliance, C (which differs only slightly from the uniaxial creep compliance, D), is shown because it is this compliance that is used in the crack growth theory discussed in the next subsection.

The thickness of the grain boundary phase (b-a in Fig. 3) divided by the grain size (the mean diameter b+a in Fig. 3) may be expressed in terms of the grain (particle) volume fraction v_g (=V_p). We find that this ratio, denoted by h, is

$$h = (1 - v_g^{1/3})/(1 + v_g^{1/3}) \qquad (7)$$

For the values of v_g = .9, .99, .999 (used in Figs. 4 and 5), we find, respectively, h =.018, .0017, .00017; these values are believed to cover a realistic range for ceramics [2]. Similarly, the ratio of initial Young's modulus of the amorphous grain boundary phase to that for the grains in actual ceramics is likely to be in the range from 1/5 to unity; these are the values used for Figs. 4 and 5 respectively.
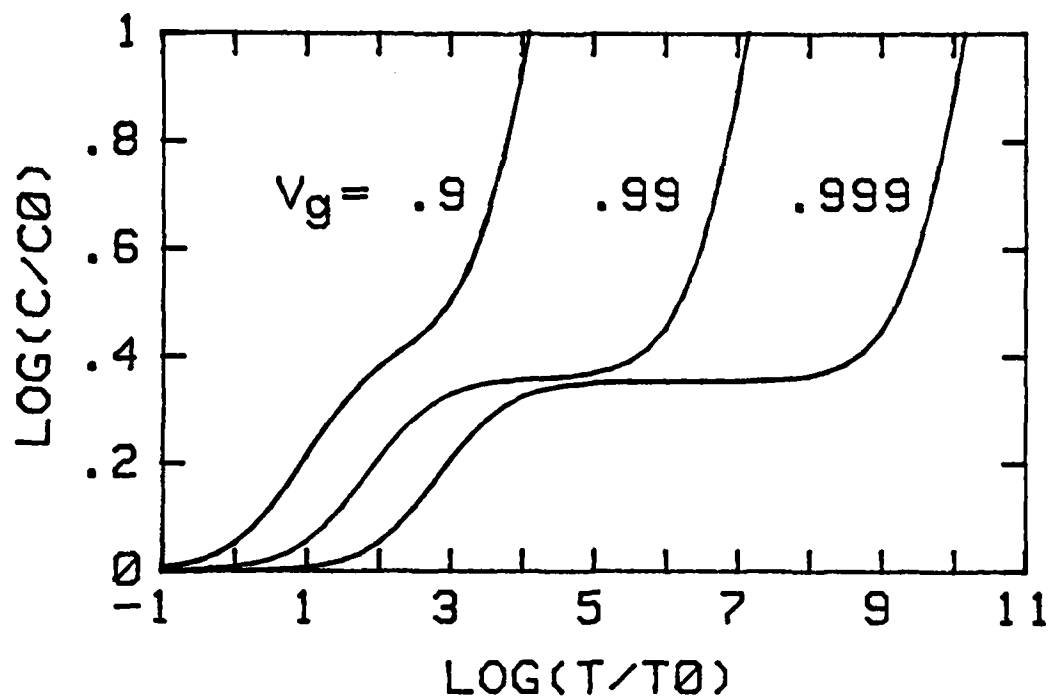
Fig. 4. Plane-strain creep compliance vs. time for three different values of the grain volume fraction. The initial Young's modulus of the grain boundary phase is 1/5 of that for the grains.
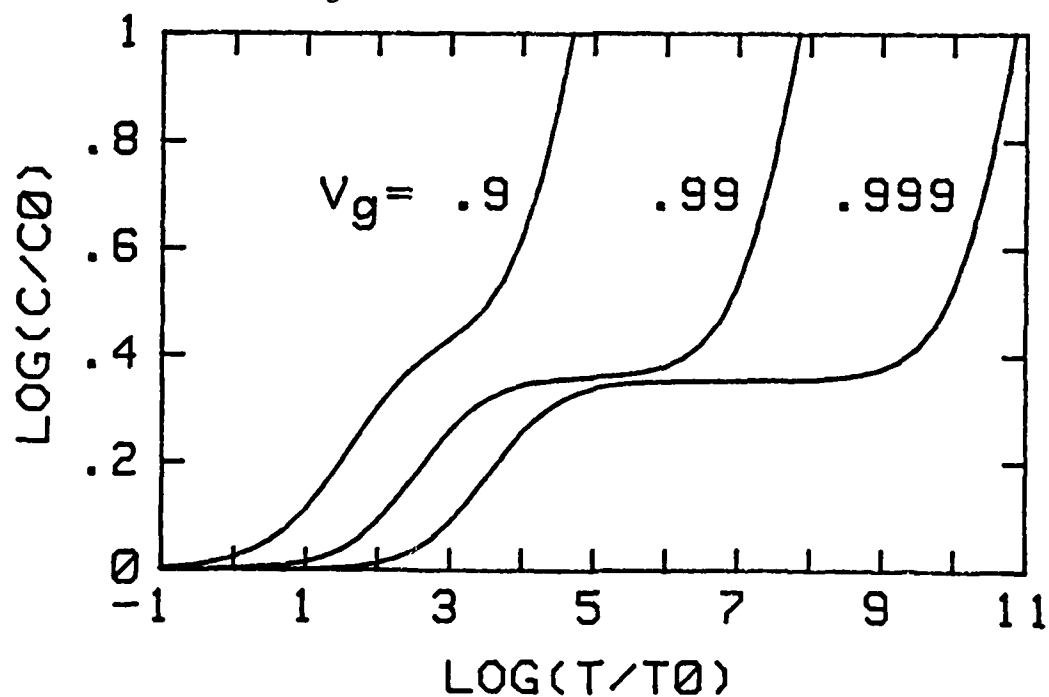

Fig. 5. Same as Fig. 4 except the initial Young's modulus of the grain boundary phase is equal to that for the grains.

Predictions of C/C_0 as a function of initial Poisson's ratios for both phases were found to be practically independent of them over the range from zero to one-half; the value of 0.3 was used for both phases in these figures. As noted earlier, the grains are assumed elastic, with constant values of Poisson's ratio and Young's modulus.

At very long times, all curves in Figs. 4 and 5 have a slope of unity (viz. $C \sim t$) as expected, since the deformation is dominated by viscous flow of the grain boundary phase; this is the behavior assumed in the crack growth theory [3]. It should be added that the long-time shear viscosity η_c, say, for the ceramic may be found using the theory in [7],

$$\eta_c \cong \dot{\eta}_m/32h^3 \qquad (8)$$

when $h \ll 1$.

Especially interesting is the short and intermediate time behavior of the creep compliance. For $v_g = .99$ and $.999$ there is a distinct elastic plateau for which $C/C_0 \cong 2.3$. In all cases, at short times there is a nearly constant slope region in which slope $\cong 0.2$, which implies $C \sim t^{0.2}$. The main difference between the results in Figs. 4 and 5 is a time-shift. Events in Fig. 4 occur about four times faster than those in Fig. 5, assuming the time constant T_0 is the same for all cases.

The viscoelastic behavior, $C \sim t^{0.2}$, and elastic behavior where $C/C_0 \sim 2.3$, stem from elastic distortions of the grains as they interact with the grain boundary phase. One has to wait a relatively very

long time until C ~ t, when the grains behave as relatively rigid particles in a viscous matrix. The insensitivity of the ceramic's creep compliance to Poisson's ratios of the phases implies insensitivity to the bulk moduli of the grains and the amorphous grain boundary phase.

In real ceramics the thickness of the grain boundary phase is expected to vary from grain-to-grain. This implies one may have to account for a distribution of local volume fractions v_g, which would lead to compliance curves that are combinations of those in Figs. 4 or 5. This generalization will be studied in future work.

2.2.3 Crack Growth Theory. Equation (1) gives the crack speed only when it is slow enough that events in the neighborhood of the crack tip take place in the very long time regime, C ~ t. We may now generalize the theory to allow for behavior over the entire time range of response shown in Figs. 4 and 5 by drawing upon Schapery's theory in [4] using the idealized crack tip model in Fig. 6.
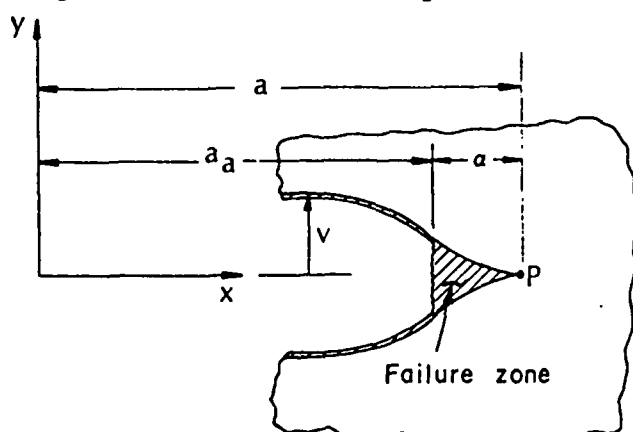

Figure 6. Cross-section of an idealized crack used in [4]. The failure zone here is to be identified with the damage zone in Fig. 1 (i.e. the cavities in a viscous layer plus the adjacent rigid grains.

The "failure zone" in this figure is to be identified with the damage zone of Fig. 1, which consists of rigid grains and a cavitating viscous layer. The theory in [4] permits us to use mechanical properties for the failure zone which are different from the surrounding ceramic continuum. The length of the failure zone α is related to the stress intensity factor K_I according to [4, Part I],

$$\alpha \sim K_I^2/\sigma_f^2 \qquad (9)$$

where σ_f is a measure of the normal stress acting across the failure (or damage) zone. From [4, Part II] the crack opening displacement at the left end of the failure zone in Fig. 6 is

$$\Delta v \sim C(t_\alpha) \, K_I^2/\sigma_f \qquad (10)$$

where C is the plane-strain creep compliance for the ceramic continuum discussed earlier, and

$$t_\alpha \cong \alpha/3\mathring{a} \qquad (11)$$

is one-third the time elapsed when the crack grows an amount α.

The viscous crack growth theory in [3] uses a critical cavity area fraction as a crack growth criterion; according to [3, Eq. (5)], this is equivalent to a critical value of $\Delta v/\lambda$ and thus a critical value Δv_c. From Eqs. (9) - (11),

$$\Delta v_c \sim C(\alpha/3\mathring{a})K_I\sqrt{\alpha} \qquad (12)$$

For a viscous body, $C \sim \alpha/3\mathring{a}$, and if α is constant then Eq. (12) yields

$$\mathring{a} \sim K^I \qquad (13)$$

which is the same behavior as in Eq. (1).

For a power law viscoelastic ceramic,

$$C \cong (t/t_o)^n C_1 \qquad (14)$$

corresponding, say, to the short time region in Figs. 4 or 5 (for which $n \cong 0.2$) and if α is constant, then Eq. (12) gives

$$\dot{a} \sim K_I^{1/n} \qquad (15)$$

With $n = 0.2$,

$$\dot{a} \sim K_I^5 \qquad (16)$$

It was assumed in [3] and in developing Eqs. (13)-(16) that α is constant. However, this is not necessarily correct. Equation (9) must be satisfied (in order that the crack-tip stress not be infinite). If we suppose that all geometric parameters at the crack tip are constant (except possibly for α) then for a viscous failure zone $\sigma_f \sim \dot{a}$, which yields

$$\alpha \sim K_I^2/\dot{a}^2 \qquad (17)$$

Substitute this behavior into Eq. (10) after using Eq. (14) to find

$$\dot{a} \sim K_I^p \qquad (18)$$

where

$$p = \frac{2n + 2}{3n + 1} \qquad (19)$$

For $n = 1$, then $p = 1$ as before; this result and Eq. (17) imply α is indeed constant. However, if $n \neq 1$, α will vary with K_I. For an elastic material, $n = 0$,

$$\dot{a} \sim K_I^2 \qquad (20)$$

whereas if $n = 0.2$,

$$\dot{a} \sim K_I^{1.5} \qquad (21)$$

which gives an exponent that is at the midpoint between elastic and viscous behavior! It should be noted that the grain boundary phase is viscous in [3] but viscoelastic in Eq. (5) and Figs. 4 and 5. For $T/T_0 > 10$, the elastic strain is negligible and therefore the two theories are for viscous behavior, $J_m \sim t$, over most of the time scale in these figures.

A more detailed analysis leads to explicit dependence of $\mathring{a}$ on the various physical and geometric parameters appearing in the cavitation model in [3]. This work will be published in the near future.

2.2.4 <u>Distributed Damage Model</u>. The value of the exponent p has a significant effect on the overall creep strain rate of a ceramic with growing microcracks, each of which obeys Eq. (18). In order to use the results in [2] for ceramics which are elastic (except for the effect of damage growth) we suppose the linear viscoelastic compliance is in the elastic plateau range of Figs. 4 and 5 (for $v_g \geq$ 0.99, say). Then, using the short-time strain rate (due to damage) from [2],

$$\dot{\epsilon} \sim \sigma^{p+1} \qquad (22)$$

and with $p \sim 1.5$,

$$\dot{\epsilon} \sim \sigma^{2.5} \qquad (23)$$

Whereas if even shorter effective times apply to the crack tip region, we use elastic behavior, and therefore $p = 2$ and

$$\dot{\epsilon} \sim \sigma^3 \qquad (24)$$

The time scale for the compliance around the damage zone is

$t_\alpha \sim \alpha/3\mathring{a}$, which is smaller than the time scale for global behavior. It is thus appropriate to select for p the slope at times less than those in the plateau.

The dark dashed lines in Fig. 2 correspond to Eq. (22) for either elastic behavior, $p + 1 = 3$, or viscoelastic behavior, $p + 1 = 2.5$. The experimental data do not all have the same slope, which may be due to, at least in part, the complexity of the creep compliance of a polycrystalline ceramic and locally varying grain volume fraction v_g.

2.2.5 Conclusions. These results on crack and damage growth are very encouraging as the viscoelasticity theory leads to internally consistent models and realistic predictions, all expressed in terms of basic micromechanisms. It is not limited to constant stress conditions. Indeed, the theory predicts strong frequency effects for crack and damage growth in cyclic loading, such as reported by Han and Suresh [8]. Future work will fill in details of this approach in order to relate response explicitly to micromechanical parameters and to different types of loading and thermal histories. Also, the applicability of the author's earlier work on distributed damage growth in particulate composites [9] and a low temperature ceramic (ice) [10] will be studied.

3. REFERENCES

[1] R.A. Schapery and B.D. Davidson, "Prediction of Energy Release Rate for Mixed-Mode Delamination Using Classical Plate Theory," Appl. Mech. Rev., 43, 1990, pp. 281-287.

[2] S. Suresh and J.R. Brockenbrough, "A Theory for Creep by Interfacial Flaw Growth in Ceramics and Ceramic Composites," Acta Metall. Mater., 38, 1990, pp. 55-68.

[3] M.D. Thouless, C.H. Hsueh and A.G. Evans, "A Damage Model of Creep Crack Growth in Polycrystals," Acta Metall., 31, 1983, pp. 1675-1687.

[4] R.A. Schapery, "A Theory of Crack Initiation and Growth in Viscoelastic Media," 11, 1975. Part I, pp. 141-159; Part II, pp. 369-388; Part III, pp. 549-562.

[5] R.M. Christensen, Mechanics of Composite Materials, Wiley, New York, 1979.

[6] R.A. Schapery, "Stress Analysis of Viscoelastic Composite Materials," J. Comp. Mat. 1, 1967, pp. 228-267.

[7] R.A. Schapery, "A Micromechanical Model for Nonlinear Viscoelastic Behavior of Particle-Reinforced Rubber with Distributed Damage," Eng'g Fracture Mech., 25, 1986, pp. 845-867.

[8] L.X. Han and S. Suresh, "High-Temperature Failure of an Alumina-Silicon Carbide Composite under Cyclic Loads: Mechanisms of Fatigue Crack-Tip Damage," J. Am. Ceram. Soc., 72, 1989, pp. 1233-1238.

[9] R.A. Schapery, "On Viscoelastic Deformation and Failure Behavior of Composite Materials with Distributed Flaws," 1987 Advances in Aerospace Strudctures and Materials, Vol. AD-01, ASME, 1981, pp. 5-20.

[10] R.A. Schapery, "Models for Deformation Behavior of Viscoelastic Media with Distributed Damage and Their Applicability to Ice," Proc. IUTAM/IAHR Symposium on Ice/Structure Interaction, St. John's Newfoundland, 1989.

4. AFOSR SPONSORED PUBLICATIONS (1990)

[1] R.A. Schapery and B.D. Davidson, "Prediction of Energy Release Rate for Mixed-Mode Delamination Using Classical Plate Theory," Appl. Mech. Rev., 43, 1990, pp. 281-287.

[2] R.A. Schapery, "A Theory of Mechanical Behavior of Elastic Media with Growing Damage and Other Changes in Structure," J. Mech. Phys. Solids, 38, 1990, pp. 215-253.

5. PROFESSIONAL PERSONNEL INFORMATION

5.1 List of Professional Personnel

R.A. Schapery, Principal Investigator
M.C. Lu, Co-Principal Investigator

5.2   Interactions (coupling activities) of the Principal Investigator

<u>Spoken Papers and Lectures</u>

1.   Paper given at Eleventh U.S. National Congress of Applied Mechanics, Tucson, June 1990: "Prediction of Energy Release Rate for Mixed-Mode Delamination Using Classical Plate Theory."

2.   Paper given at USAF Workshop on Solid Propellant, Edwards Air Force Base, CA, October 1989: "Damage Growth in Solid Propellant."

3.   Paper given at IUTAM Symposium on Inelastic Deformation of Composite Materials, Troy, NY, May 1990: "Simplifications in the Behavior of Viscoelastic Composites with Growing Damage."

4.   Lecture at NASA meeting on structural behavior of high-altitude balloons, Va, April 1990: "Application of the J Integral to Polyethylene Film."

<u>Additional Coupling Activities</u>

1.   Participant in AFOSR Workshop on Damage Mechanics in Composite Material Design, Santa Barbara, CA, June 1990.

2.   Member of NASA Advisory Panel on High-Altitude Balloons (1988-present).

APPENDIX

Prediction of Energy Release Rate
for Mixed-Mode Delamination
Using Classical Plate Theory

Prediction of energy release rate for mixed-mode delamination using classical plate theory

R A Schapery

Civil Engineering Deoartment, Texas A&M University, College Station TX 77843

B D Davidson

*Mechanical Systems Egineering and Research Division, Jet Propulsion Laboratory,
Pasadena CA 91109*

Prediction of the energy release rate (ERR) and its components for mixed-mode delamination of composite laminates is discussed. A classical plate theory (CPT) version of Irwin's virtual crack closure method is developed and used for the ERR, first for plane strain and then for three-dimensional deformations. It is shown that CPT does not provide quite enough information to obtain a decomposition of ERR into its opening and shearing mode components. Results from a continuum analysis are needed to complete the decomposition; but analysis of only one loading case is required for two-dimensional and certain three-dimensional problems. In two example problems the finite element method is used with CPT to complete the mode decomposition. Results from CPT and the finite element method are then compared for several cases.

1. INTRODUCTION

Delamination is a commonly occurring type of crack growth in many composite laminates . The strength and stiffness of a composite structure may be significantly affected by delamination, whether the loading is in-plane or out-of-plane. One indication of the importance of the delamination problem, especially for fiber-reinforced plastics, is the large number of publications devoted to the subject, such as found in a recent book on fracture of composites (Friedrich, 1989). The energy release rate (ERR) is the loading parameter commonly used to characterize the initiation and continuation of crack growth. Delamination growth in many composites depends on not only the (total) ERR but also on how much energy is in the shearing- and opening-mode components. Numerous experimental studies (e.g. Johnson and Mangalgiri, 1987) have shown that the ERR required for delamination growth varys with the ratio of shearing-to-opening mode components of the ERR; the sensitivity to this mode-ratio appears to be least in the toughest composites. To predict initiation of growth, one compares the available and required values of ERR, while stable growth rate is usually expressed in terms of the available ERR; the amplitude of ERR is often used for cyclic loading.

In this paper we are concerned with the prediction of ERR and its components in terms of the loading acting on a laminate. For use with cyclic loading problems, the ERR amplitude and its components may be found from the theory. There is no fundamental restriction on the geometry of the laminate, which may be a plate, shell or beam. The problem may, for example, be

that of predicting edge delamination in a uniaxial tensile specimen, Fig. 1, or growth of an embedded delamination in a plate under in-plane compression or a transverse load, Fig. 2. Problems like the latter one often involve geometric nonlinearities due to the out-of-plane deformations; what is developed here can be used even with geometric nonlinearities.

The approach consists of analyzing only the neighborhood of a short segment of the delamination edge; the cross-section of the near-edge region is illustrated in Fig. 3, in which there is one delamination or crack of length "a" within this element. In general, the delamination edge is a curve which may be open and thus end at the edges of the laminate (e.g. Fig. 1) or closed (e.g. Fig. 2). The x-axis in Fig. 3 is located at the midsurface and is normal to the local delamination edge. We shall call the geometry in Fig. 3 a crack tip element. The length of this element perpendicular to the plane of the page (the y-direction) is denoted by L_y; it is assumed to be short enough that there is no significant variation in the loading and the edge's orientation with respect to y. It is further assumed that (a,b) >> t, but yet a and b are small enough that geometric nonlinearities are negligible, given the moments and forces acting on this element. In order to predict loading on the element (from an overall plate or shell analysis) it may be necessary to account for geometric nonlinearities and possibly other complicating factors such as shear deformations. However, for the crack tip element itself, we assume classical linear, elastic plate theory (CPT) may be used to predict deformations

Appl Mech Rev vol 43, no 5, Part 2, May 1990
S281 © Copyright 1990 American Society of Mechanical Engineers
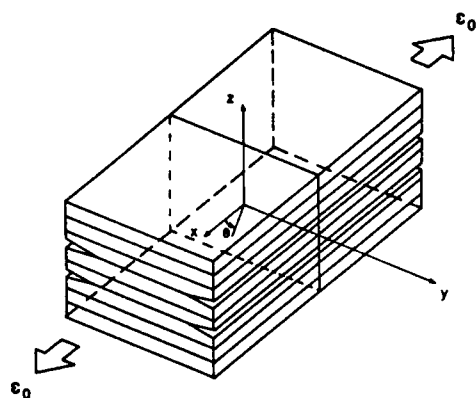
FIG. 1.   Eight ply laminate with edge delaminations. (After Raju et al., 1988).
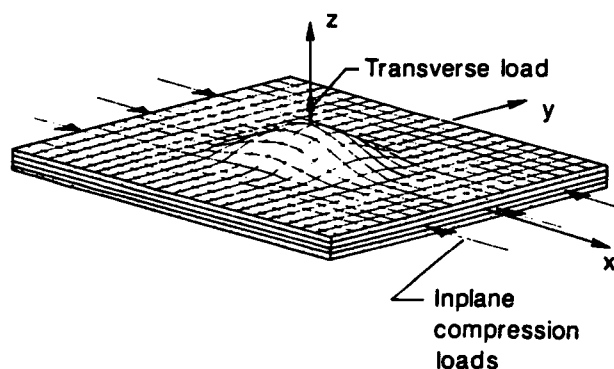

FIG. 2.   Locally postbuckled laminate with embedded delamination. (After Whitcomb and Shivakumar, 1989).
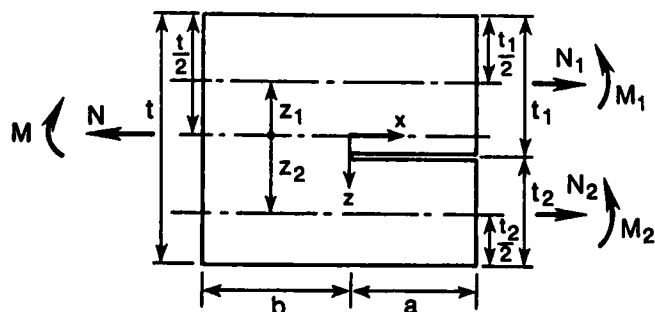

FIG. 3.   Crack tip element for plate theory showing loading and dimensions.

and strain energies. In CPT the deformations are defined entirely by midsurface strains and curvatures; external forces which are normal to the midsurface and act at locations away from this element are fully accounted for through the loads parallel to the midsurface and the moments. The ERR for this element is the work (divided by $L_y \delta a$) that becomes available at the crack tip when the crack advances a distance δa along the length L_y.

Essentially the same considerations have been used by Storakers and Andersson (1988), Whitcomb (1989), Whitcomb and Shivakumar (1989) and Williams (1988) to derive the ERR. In addition, Williams (1988) decomposed the ERR into opening and shearing components; however, it was assumed that a pure opening mode exists when the only loading is $M_1 = -M_2$, which we show later is not generally true. In order to determine the components of ERR, Whitcomb (1984, 1986) used finite element solutions with the virtual crack closure method.

In this paper we express the ERR directly in terms of the one concentrated moment and two components of shearing force which act at the delamination edge. These three reactions are easily written in terms the various loads and moments which act on the boundaries of the crack tip element. By using crack-tip reactions, we obtain immediately the CPT version of ERR components. Also, the connection between these components and the true ERR components based on a local continuum analysis of the crack tip is readily established in terms of the smallest possible number of independent inputs. To the authors' knowledge, none of the other publications which use CPT (including that of Davidson (1988), which is a forerunner to the present analysis) express the ERR in terms of crack tip forces and moment. Instead, in these other works the ERR is written in terms of the several forces and moments which act on the boundary of the crack tip element.

In Section 2 the ERR is derived for a state of plane strain. The theory is extended to three-dimensional deformations in Section 3. Section 4 gives examples using CPT and corresponding finite element predictions. The finite element model employed is described in the appendix.

2.   PLANE STRAIN CRACK TIP ANALYSIS

Plate Equations

Assuming a state of plane strain for now, and referring to Fig. 3, we consider only the inplane loads N, N_1 and N_2 and moments M, M_1 and M_2; these quantities are resultants per unit of length in the y-direction, and are positive when they act in the directions shown. From overall equilibrium of the geometry in Fig. 3 and observing that $z_1 = -t_2/2$ and $z_2 = t_1/2$,

$$N = N_1+N_2, \quad M = M_1+M_2+N_2 t_1/2 - N_1 t_2/2 \qquad (1)$$

The energy release rate is expressed most simply in terms of the crack tip shear force N_c and moment M_c, Fig. 4. The presence of a crack tip is fully accounted for by concentrated reactions N_c and M_c because, in the context of CPT, there are no tractions which act across the surface of crack prolongation in the uncracked
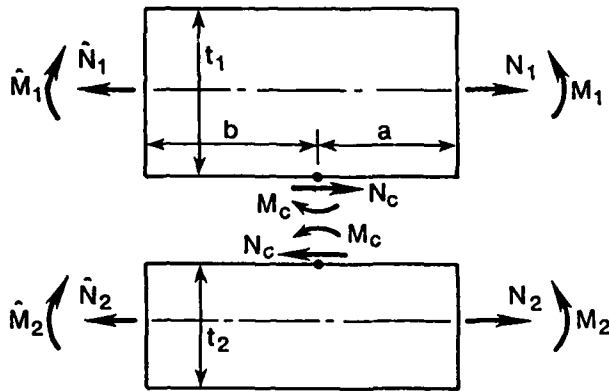
FIG. 4. Free body diagram for plates above and below the crack plane.

section, and the deformation depends only upon moments and axial forces. Considering the top free-body in Fig. 4,

$$N_c = -N_1 + \hat{N}_1 \tag{2}$$

$$M_c = M_1 + N_c t_1/2 - \hat{M}_1 \tag{3}$$

The quantities $\hat{N}_1$ and $\hat{M}_1$ are internal stress-resultants in the uncracked section. They may be found from CPT and expressed in terms of the overall force N and moment M in this section, Fig. 3, as follows. Using Jone's (1975) notation, for the full laminate,

$$N = A\varepsilon^o + B\kappa \tag{4a}$$

$$M = B\varepsilon^o + D\kappa \tag{4b}$$

where ε^o is the midsurface (z=0) strain and κ is the curvature. Also, A, B and D are the extensional stiffness, coupling stiffness, and bending stiffness, respectively. Similarly, for the laminate or material "1" above the crack plane, but in the uncracked section,

$$\hat{N}_1 = A_1 \varepsilon^o_{1u} + B_1 \kappa = A_1 \varepsilon^o + (B_1 - A_1 t_2/2)\kappa \tag{5a}$$

$$\hat{M}_1 = B_1 \varepsilon^o_{1u} + D_1 \kappa = B_1 \varepsilon^o + (D_1 - B_1 t_2/2)\kappa \tag{5b}$$

where we have used the fact that the midsurface strain for material "1" is

$$\varepsilon^o_{1u} = \varepsilon^o + z_1 \kappa = \varepsilon^o - \kappa t_2/2 \tag{6}$$

Now, write the inverse of Eq. (4) as

$$\varepsilon^o = A'N + B'M \tag{7a}$$

$$\kappa = B'N + D'M \tag{7b}$$

in which the primed quantities are compliances. Use this result in Eq. (5) to obtain the desired force and moment,

$$\hat{N}_1 = a_{11}N + a_{12}M \tag{8a}$$

$$\hat{M}_1 = a_{21}N + a_{22}M \tag{8b}$$

where

$$a_{11} = A_1 A' + (B_1 - A_1 t_2/2)B'$$

$$a_{12} = A_1 B' + (B_1 - A_1 t_2/2)D'$$

$$a_{21} = B_1 A' + (D_1 - B_1 t_2/2)B'$$

$$a_{22} = B_1 B' + (D_1 - B_1 t_2/2)D' \tag{9}$$

Equations (2) and (3) become

$$N_c = -N_1 + a_{11}N + a_{12}M \tag{10}$$

$$M_c = M_1 - N_1 t_1/2 + (a_{11}t_1/2 - a_{21})N + (a_{12}t_1/2 - a_{22})M \tag{11}$$

Energy Release Rate

A plate theory version of Irwin's (1957) virtual crack closure method will be used to derive the energy release rate. First, we consider the crack tip to be just inside the left edge of the geometry in Fig. 3. The left edge is then the right boundary of the uncracked plate, and may be treated as a fixed edge. Now, referring to Fig. 4 with N_c and M_c initially zero, gradually increase them until they have the values needed to close the crack along the length b; these values are given by Eqs. (10) and (11). The work of crack closing divided by b is also the ERR, G, when the crack length grows any small amount b. Thus,

$$G = \frac{1}{2b} (N_c \Delta u + M_c \Delta \theta) \tag{12}$$

where $\Delta u = u_1 - u_2$ and $\Delta \theta = \theta_2 - \theta_1$. The u_i and θ_i refer to horizontal displacement and rotation of the crack surfaces for the top (i=1) and bottom (i=2) plates due only to N_c and M_c. Namely, with the left edge fixed,

$$u_1 = b(\varepsilon_1 + \kappa_1 t_1/2), \quad \theta_1 = \kappa_1 b \tag{13a}$$

$$u_2 = b(\varepsilon_2 - \kappa_2 t_2/2), \quad \theta_2 = \kappa_2 b \tag{13b}$$

where ε_i and κ_i are midsurface strain and curvature, respectively, due to N_c and M_c.

For the material above the crack plane the stiffness matrix has components A_1, B_1 and D_1, as in Eq. (5). We may derive the midsurface strain and curvature using the inverse of the stiffness matrix (A_1', B_1', D_1') and, as inputs, the midsurface load and moment shown in Fig. 5; thus

$$\varepsilon_1 = A_1'N_c + B_1'(N_c t_1/2 - M_c) \tag{14a}$$

$$\kappa_1 = B_1'N_c + D_1'(N_c t_1/2 - M_c) \tag{14b}$$

Substitution of Eq. (14) and analogous results for the material below the crack surface into Eq. (13) yields, finally,

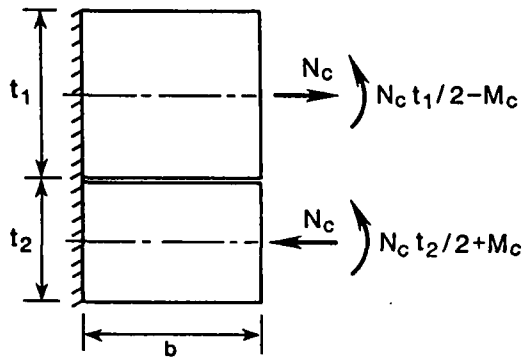$$\Delta u/b = c_1 N_c + c_{12} M_c \tag{15a}$$

FIG. 5. Loading on plates above and below the crack plane which is statically equivalent to loading at the crack tip.

$$\Delta\theta/b = c_{12}N_c + c_2 M_c \qquad (15b)$$

where

$$c_1 = A_1' + A_2' + B_1' t_1 - B_2' t_2 + D_1' t_1^2/4 + D_2' t_2^2/4 \qquad (16a)$$

$$c_2 = D_1' + D_2' \qquad (16b)$$

$$c_{12} = D_2' t_2/2 - D_1' t_1/2 - B_1' - B_2' \qquad (16c)$$

and the subscripts 1 and 2 on (A', B', D') refer to the plate properties above and below the crack plane, respectively. From Eqs. (12) and (15), the ERR becomes

$$G = \frac{1}{2} (c_1 N_c^2 + c_2 M_c^2 + 2c_{12} N_c M_c) \qquad (17)$$

Given that $G > 0$ for N_c and M_c not both zero, it follows that $c_1 > 0$, $c_2 > 0$ and $c_1 c_2 > c_{12}^2$.

Mode Decomposition

For those cases in which the stresses in the continuum in the neighborhood of the crack tip exhibit the behavior $r^{-1/2}$, where r is distance from the tip, we may write

$$G = G_I + G_{II} \qquad (18)$$

where G_I and G_{II} are the mode I (opening mode) and mode II (shearing mode) energy release rates. In turn $G_I \sim K_I^2$ and $G_{II} \sim K_{II}^2$, where K_I and K_{II} are the associated stress intensity factors. These factors are real, linear functions of the loads which produce crack-tip stresses; the crack tip loading here is defined entirely by N_c and M_c. Thus, we may write Eq. (17) in the form

$$2G = g_1^2 + g_2^2 \qquad (19)$$

where

$$g_1 \equiv (2G_I)^{1/2} = k_1 N_c + k_2 M_c \qquad (20a)$$

$$g_2 \equiv (2G_{II})^{1/2} = k_3 N_c + k_4 M_c \qquad (20b)$$

and the k_i are real coefficients. If the k_i are known, the G_I and G_{II} components of ERR may be calculated in terms of external loads and moments through N_c and M_c, Eqs. (10) and (11).

Thus, it only remains to find the four k_i. By equating G in Eq. (19) to Eq. (17) and matching the coefficients of N_c^2, M_c^2 and $N_c M_c$ we find

$$k_2 = [c_{12}k_1 + s_2(c_1 - k_1^2)^{1/2}c]/c_1 \qquad (21a)$$

$$k_3 = s_3(c_1 - k_1^2)^{1/2} \qquad (21b)$$

$$k_4 = (c_{12} - k_1 k_2)/k_3 \qquad (21c)$$

where $s_2 = \pm 1$, $s_3 = \pm 1$ and

$$c = (c_1 c_2 - c_{12}^2)^{1/2} \qquad (21d)$$

The sign s_3 determines the sign of both k_3 and k_4, and since these coefficients define the sign of K_{II} (and g_2) we may use $s_3 = 1$ without any real loss in generality. For the cases studied numerically to-date

$$c_{12}k_1 < (c_1 - k_1^2)^{1/2}c \qquad (22)$$

and thus we must use $s_2 = 1$ so that $k_2 > 0$; according to Eq. (20a), if $k_2 < 0$ a sufficiently large positive crack tip moment would produce the physically unacceptable result of a negative opening-mode stress intensity factor.

There is not enough information available from CPT to find the one remaining unknown coefficient k_1. As k_1 is independent of the loading, we may use numerical or other results from an analysis of any one special loading case. It is helpful to select applied moments and loads which make $N=M=0$. In this case Eqs. (1), (10) and (11) yield

$$N_2 = -N_1, \qquad M_2 = -M_1 + N_1 t/2 \qquad (23)$$

$$N_c = -N_1, \qquad M_c = M_1 - N_1 t_1/2 \qquad (24)$$

Further, if $N_1 = 0$ then $M_2 = -M_1$, $N_c = 0$ and $M_c = M_1$. Alternatively, if $M_1 = N_1 t_1/2$ then $M_c = 0$ and $M_2 = N_1 t_2/2$. In the latter case Eq. (20a) reduces to $g_1 = -k_1 N_1$, so that if g_1 is known for this one loading case,

$$k_1 = -g_1/N_1 \qquad (25)$$

Nondimensionalization

Here we shall rewrite the primary variables and equations in dimensionless form to allow for thickness and modulus scaling.

Let E and T be the reference modulus and thickness, respectively. Then, with an asterisk used to denote a nondimensionalized variable, we write for stiffnesses,

$$A^* = A/ET, \quad B^* = B/ET^2, \quad D^* = D/ET^3 \qquad (26)$$

compliances,

$$A'^* = A'ET, \quad B'^* = B'ET^2, \quad D'^* = D'ET^3 \qquad (27)$$

load and moment,

$$N^* = N/ET, \qquad M^* = M/ET^2 \qquad (28)$$

and thickness and curvature,

$$t^* = t/T, \qquad \kappa^* = \kappa T \qquad (29)$$

where the subscript "1" or "2" may be used with the variables in Eqs. (26)-(28), as appropriate. The energy release rate and related variables are

$$G^* = G/ET, \qquad (30)$$

$$c_1^* = c_1 ET, \quad c_2^* = c_2 ET^3, \quad c_{12}^* = c_{12} ET^2 \qquad (31)$$

$$g_i^* = g_i/(ET)^{1/2} \quad \text{for } i = 1,2 \qquad (32)$$

$$k_i^* = k_i(ET)^{1/2} \quad \text{for } i = 1,3 \qquad (33)$$

$$k_i^* = k_i(ET)^{1/2}T \quad \text{for } i = 2,4 \qquad (34)$$

The ERR in terms of the dimensionless variables is the same as that in Eq. (17),

$$G^* = \frac{1}{2}\,[c_1^*(N_c^*)^2 + c_2^*(M_c^*)^2 + 2c_{12}^*\, N_c^*\, M_c^*] \qquad (35)$$

and the equations for the coefficients are the same as in Eq. (16), e.g.

$$c_2^* = D_1'^* + D_2'^* \qquad (36)$$

Similarly, just as in Eq. (20),

$$g_1^* = k_1^* N_c^* + k_2^* M_c^* \qquad (37)$$

We may use these results by finding solutions for k_i^* using E=T=1 and then generalizing the results to arbitrary E and T by means of Eqs. (33) and (34); e.g.

$$k_1 = k_1^*/(ET)^{1/2} \qquad (38)$$

Homogeneous, Isotropic Plates

In the numerical examples in Section 4 the split plate is assumed to be made of one or two homogeneous, isotropic materials. For this case the stiffnesses are (Jones, 1975),

$$A_i = E_i t_i/(1-\nu_i^2), \quad B_i = 0, \quad D_i = E_i t_i^3/12(1-\nu_i^2) \quad (39)$$

where ν_i and E_i are Poisson's ratio and Young's modulus, respectively. The compliances are

$$A_i' = 1/A_i, \quad B_i' = 0, \quad D_i' = 1/D_i \qquad (40)$$

and the ERR coefficients are

$$c_1 = 4\left[\frac{1-\nu_1^2}{E_1 t_1} + \frac{1-\nu_2^2}{E_2 t_2}\right] \qquad (41)$$

$$c_2 = 12\left[\frac{1-\nu_1^2}{E_1 t_1^3} + \frac{1-\nu_2^2}{E_2 t_2^3}\right] \qquad (42)$$

$$c_{12} = 6\left[\frac{1-\nu_2^2}{E_2 t_2^2} - \frac{1-\nu_1^2}{E_1 t_1^2}\right] \qquad (43)$$

Observe that $c_{12} = 0$ when the top and bottom plates are identical. Also, plane stress results

are obtained by omitting the ν_i^2 terms.

3. THREE-DIMENSIONAL CRACK TIP ANALYSIS

We continue to use the crack tip element in Fig. 3, but now allow for three in-plane shear forces in the y-direction (say N_1^y, N_2^y, N^y) which act on the same three areas as N_1, N_2 and N. It is assumed that $L_y \gg b \gg t$, where L_y is the element length in the y-direction, but that L_y is small enough for all loads and moments to be essentially independent of y over L_y.

A crack tip shear force in the y-direction, say N_c^y, also may exist. Similar to Eq. (2), we obtain

$$N_c^y = -N_1^y + \hat{N}_1^y \qquad (44)$$

In order to find $\hat{N}_1^y$ as well as $\hat{N}_1$ and $\hat{M}_1$ for use in Eqs. (2) and (3), the full three-dimensional plate equations are needed. In place of Eqs. (4) and (5) use equations of the type (Jones, 1975),

$$\begin{Bmatrix} N \\ M \end{Bmatrix} = \begin{bmatrix} A & B \\ B & D \end{bmatrix} \begin{Bmatrix} \varepsilon^0 \\ \kappa \end{Bmatrix} \qquad (45)$$

where each of the terms $N, M, \varepsilon^0, \kappa$ represents a set of three components (e.g. N_x, N_y, N_{xy}), and each element A, B and D represents a 3×3 symmetric matrix. As before, one set of equations is needed for the full laminate and one set is needed for the material above the crack plane.

The ERR is now

$$G = \frac{1}{2b}\,(N_c \Delta u + M_c \Delta\theta + N_c^y \Delta v) \qquad (46)$$

where $\Delta v = v_1 - v_2$ is the difference between y-displacements across the crack plane due to N_c, M_c and N_c^y. In place of Eq. (15), use

$$\Delta u/b = c_1 N_c + c_{12} M_c + c_{13} N_c^y \qquad (47a)$$

$$\Delta\theta/b = c_{12} N_c + c_2 M_c + c_{23} N_c^y \qquad (47b)$$

$$\Delta v/b = c_{13} N_c + c_{23} M_c + c_3 N_c^y \qquad (47c)$$

where the c's are found using a procedure which is the same as for the plane strain case. It should be noted that the constraint of the uncracked material along the left edge of the plates in Fig. 4 limits the deformation caused by N_c, M_c and N_c^y to ε_x^0, κ_x and γ_{xy}^0; i.e. the c's are to be found using the special case $\varepsilon_y^0 = \kappa_y = \kappa_{xy} = 0$ in Eq. (45).

From Eqs. (46) and (47),

$$G = \frac{1}{2}\,[c_1 N_c^2 + c_2 M_c^2 + c_3 (N_c^y)^2 + 2c_{12} N_c M_c$$

$$+ 2c_{13} N_c N_c^y + 2c_{23} M_c N_c^y] \qquad (48)$$

When there is no coupling between the force N_c^y and the cross-sectional variables Δu and $\Delta\theta$ (i.e. $c_{13} = c_{23} = 0$) then G is the same as in Eq. (17) except for the additional term

$c_3(N_c^y)^2$. In this case, and without (x,y) coupling of the stress singularities, the opening and shearing mode components (in the x-z plane) of ERR depend only on N_c and M_c, and may be found from Eq. (20) using the coefficients for plane strain. The antiplane shearing component of G is then simply $c_3(N_c^y)^2/2$.

With full coupling there are nine coefficients k_i in the three-dimensional version of Eq. (20), in which the g_i (i=1,2,3) are expressed in terms of N_c, M_c, and N_c^y. Equation (48) may be used, as in the plane strain case, to solve for six k_i in terms of the remaining three. However, it might be easier to use a method similar to Whitcomb's (1984) approach; three different loading cases (to obtain three different sets of N_c, M_c and N_c^y) would be analyzed by the finite element method to find the nine k_i.

4. EXAMPLES

Two-Layer Plate

Consider a crack between two different homogeneous isotropic plates of equal thickness, for which we select $t_1 = t_2 = 1$, $E_1 = 1$, $E_2 = 1.923$, $v_1 = 0.3$, $v_2 = 0$. For plane strain and these values of Poisson's ratio and modulus the stress singularity at the crack tip is real (Raju et al., 1988) and thus does not have the oscillatory character common to cracks between dissimilar media.

Equations (41)-(43) provide the coefficients in the ERR, Eq. (17); we find that

$$G = \frac{1}{2}(5.72\, N_c^2 + 17.2\, M_c^2 - 4.68\, N_c M_c) \qquad (49)$$

The coefficient k_1 in Eq. (20a) is found to be -0.174 from finite element analysis (cf. Appendix) and Eq. (25). The loading used for this case is $N_1 = 2$, $N_2 = -2$, $M_1 = M_2 = 1$, which yields $N_c = -2$ and $M_c = 0$. The remaining k_i are obtained from Eq. (21) to give in Eq. (20),

$$g_1 = (2G_I)^{\frac{1}{2}} = -0.174N_c + 4.09M_c \qquad (50a)$$

$$g_2 = (2G_{II})^{\frac{1}{2}} = 2.39N_c - 0.683M_c \qquad (50b)$$

Table I compares the plate predictions (P) from Eqs. (49) and (50) with values determined directly from the finite element model (F) for several different loading cases in which N_1, N_2, M_1 and M_2 are varied.

TABLE I. ERR COMPARISONS FOR THE TWO-
LAYERED PLATE
===

Case	N_c	M_c	G_P	G_F	$\frac{G_I}{G_{II}}_P$	$\frac{G_I}{G_{II}}_F$
1	-2	0	11.4	11.5	--	5.34×10^{-3}
2	-3.09	.152	28.6	28.6	.0240	.0240
3	-6.83	1.80	190	191	.237	.241
4	-1.78	.712	16.3	16.4	.465	.464
5	-4.39	3.22	177	177	1.21	1.21
6	-3.81	3.84	203	202	1.95	1.94
7	-1.06	1.36	22.3	22.2	2.75	2.73
8	0	1	8.58	8.57	35.8	36.0

It is seen that agreement between plate theory and finite element analysis is very good for all cases.

Homogeneous Plate

The second problem is that of a homogeneous, isotropic plate in plane strain with an off-center crack. Specifically, $t_1 = 1$, $t_2 = 0.5$, $E_1 = E_2 = 1$, $v_1 = v_2 = 0.3$. Use of Eqs. (41)-(43) and (17) yields,

$$G = \frac{1}{2}(10.9N_c^2 + 98.3M_c^2 + 32.8N_c M_c) \qquad (51)$$

Equation (25) and a finite element analysis give $k_1 = 0.398$, so that from Eqs. (20) and (21),

$$g_1 = 0.398N_c + 9.12M_c \qquad (52a)$$

$$g_2 = 3.28N_c + 3.89M_c \qquad (52b)$$

The k_1 value was found from the pure shear loading case $N_c = 2$, $M_c = 0$. One important comparison that can be made between plate theory and finite element analysis is for the other extreme case of pure moment loading. With $N_c = 0$, $M_c = 1$ we found very good agreement, in that both methods yielded G = 49.1 and $G_I/G_{II} = 5.50$. Other loading cases were analyzed, with the same conclusion.

Discussion

The many loading cases studied numerically in both problems have used a variety of values for N_1, N_2, M_1 and M_2. That the only effective crack tip loading parameters are N_c and M_c was confirmed by the agreement of the continuum analysis (using finite elements) with CPT. That CPT provides total ERR which is usually in good agreement with finite element predictions has also been reported by Whitcomb (1989) for a postbuckled, embedded delamination. The accuracy of CPT in predicting ERR thus makes it a useful tool for checking whether or not the mesh size and proportions in finite element models are acceptable.

In the two example problems the values $t_1 = E_1 = 1$ were used. By selecting $T = t_1$ and $E = E_1$ in the earlier section on nondimensionalization we may convert the calculated k_i and c_i values, which may be interpreted as k_i^* and c_i^*, to those for other moduli and thicknesses using, for example, Eq. (38).

It is of interest to observe that Eqs. (50a) and (52a) show G_I does not necessarily vanish even if the crack tip moment vanishes. Similarly, when the shear force vanishes G_{II} is not necessarily zero. Such results are possible because N_c and M_c are only resultants, and thus do not reflect details in the local stress distribution. On the other hand k_1 is relatively small in both problems, and it would be interesting to investigate whether or not $k_1 = 0$ can be used generally. If this approximation is valid, then k_2, k_3 and k_4 may be derived directly from Eq. (21), without having to use results from finite-element or other analyses. The accuracy of delamination predictions with $k_1 = 0$ depends on the delamination criterion. For example, if the critical value of G is independent of mode ratio, then any value of $k_1^* \leq c_1$ will suffice

because Eq. (21) guarantees that G, Eq. (17), is independent of k_1. Note also that symmetry yields $k_1 = k_4 = C_{12} = 0$ exactly for a symmetric laminate with a midsurface crack.

The use of $k_1 = 0$ avoids the problem of finding G_I/G_{II} from a continuum analysis when the stress singularity is oscillatory. Raju et al. (1988) have shown that G_I and G_{II} do not converge (although G does converge) with decreasing finite element mesh size; an analytically evaluated limit shows similar behavior. Thus, k_1 cannot be found for this common type of singularity at a crack tip between dissimilar media. Further study is needed to determine if the use of $k_1 = 0$ or any other real value is a valid way of avoiding the oscillatory singularity problem.

5. CONCLUSIONS

The energy release rate (ERR) has been derived for two- and three-dimensional delamination problems using classical plate theory (CPT). The plate analysis was simplified by recognizing that the three-dimensional ERR and its components can be fully determined from one moment and two shear forces at the crack tip; for two dimensions, there is only one moment and one shear force. Decomposition of the plate theory ERR into opening and shearing mode components was accomplished by combining it with numerical results from a continuum analysis; an approximation which avoids the use of any solutions beyond plate theory was proposed. Finally, good agreement between CPT and finite element predictions was shown for ERR and its components.

ACKNOWLEDGEMENT

REFERENCES

Davidson, B D (1988), Two New Techniques for Predicting Delamination Growth in Laminated Plates, PhD Dissertation, Texas A&M University (Report No. MM 9045-88-19).

Friedrich, K (1989), Application of Fracture Mechanics to Composite Materials. Composite Materials Series, 6, Elsevier, New York.

Irwin, G R (1957), Analysis of Stresses and Strains Near the End of a Crack Traversing a Plate, J. Appl. Mech., 361-364.

Johnson, W S and Mangalgiri (1987), Influence of the Resin on Interlaminar Mixed-Mode Fracture, ASTM STP 937, 295-315.

Jones, R M (1975), Mechanics of Composite Materials, McGraw-Hill, New York.

Raju, I S, Crews, J H Jr. and Aminpour, M A (1988), Convergence of Strain Energy Release Rate Components for Edge-Delaminated Composite Laminates, Eng Fracture Mech, 30, 383-396.

Storakers, B and Andersson, B (1988), Nonlinear Plate Theory Applied to Delamination in Composites, J Mech Phys Solids, 36, 689-718.

Whitcomb, J D (1984), Strain-Energy Release Rate Analysis of Cyclic Delamination Growth in Compressively Loaded Laminates, ASTM STP 836, 175-193.

Whitcomb, J D (1986), Parametric Analytical Study of Instability-related Delamination Growth, Comp Sci Techn 25, 19-48.

Whitcomb, J D (1989), Comparison of Full 3-D, Thin-Film 3-D, and Thin-Film Plate Analyses of a Postbuckled Embedded Delamination, ASTM J Comp Techn & Res 11, 154-157.

Whitcomb, J D and Shivakumar, K N (1989), Strain Energy Release Rate Analysis of Plates with Postbuckled Delaminations, J Comp Mat 23, 714-734. (Originally published as NASA TM 89091, 1987).

Williams, J G (1988), On the Calculation of Energy Release Rates for Cracked Laminates, Int J Fracture, 36, 101-119.

APPENDIX

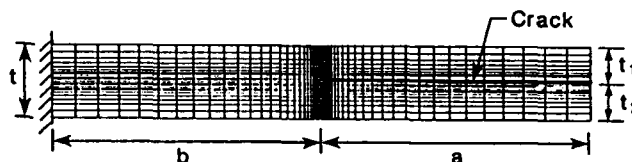Figures 6 and 7 show the finite element

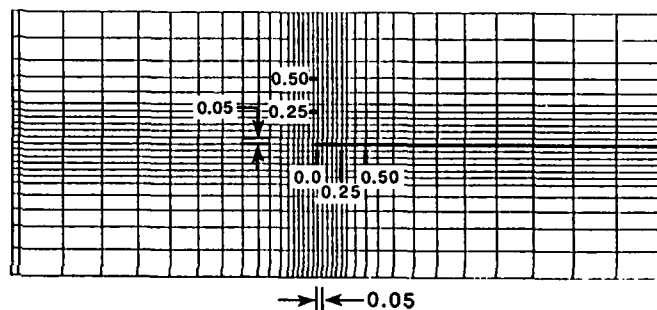FIG. 6. Finite element model used for ERR predictions.

FIG. 7. Expanded view of crack tip neighborhood.

model employed to obtain results for plane strain given in Section 4. We used four node isoparametric, quadrilateral elements in the code MSC•PAL2   Version 3.5 (The MacNeal-Schwendler Corp., Los Angeles, CA 90041) and pre- and postprocessor FEMAP Version 3.0 (Enterprise Software Products, Inc., Harleysville, Pa., 19438). The parameters t_1 and E_1 were selected as the reference thickness and reference modulus, respectively, and thus we used for calculation purposes $t_1 = E_1 = 1$. Also, a=b=10. For the case $t_2 = .5$, the same mesh as in Figs. 6 and 7 was used but the three bottom rows of elements were removed. Loads and moments were applied to the right end of the model by specifying values for four loads at the top and bottom nodes on the plates above and below the crack. Crack tip nodel forces were found by using very stiff horizontal and vertical spring elements to connect nodes across the crack plane; the displacement between these nodes was at least four orders of magnitude less than that for the adjacent crack surface nodes.

In order to determine if the mesh was fine enough to provide accurate results, additional runs were made using elements around the crack tip of size 0.01x0.01 in place of the 0.05x0.05 elements shown in Fig. 7. In most cases the change was less than one percent for G and five percent for G_I and G_{II}.